

THERMAL ASPECTS OF SELECTIVE LASER SINTERING OF PMMA+ β -TCP COMPOSITES

Rajkumar Velu and Sarat Singamneni

Additive Manufacturing Research Centre, AUT University, Auckland, New Zealand

REVIEWED

Abstract

Biocompatible and osteoconductive characteristics expected of materials used for bone grafting applications identified Polymethyl methacrylate (PMMA) and β -Tri Calcium Phosphate (β -TCP) combinations to be potential biopolymer composite options. Together with additive manufacturing methods such as selective laser sintering (SLS), these materials options would also bring about the benefits of free from fabrication. While earlier research laser sintering PMMA+ β -TCP composites experimentally proved the combination to be promising, the resulting microstructures are indicative of varied coalescence and consolidation with varying amounts of β -TCP. Considering the differential thermal properties, it becomes necessary and interesting to evaluate the possible role of the filler material in altering the nature of the thermal fields. This paper presents results of numerical and experimental work carried out investigating the thermal fields of laser sintered PMMA+ β -TCP composites.

I. Introduction

With the developments specifically in selective laser sintering (SLS) and melting (SLM), fused deposition modelling (FDM), and inkjet 3D printing (3DP) techniques, additive manufacturing (AM) gained considerable momentum in the recent years [1, 2]. While product design and industrial applications are on the rise, typical biomedical uses include surgical devices, treatments of anatomic defects, reconstruction of complex organs with intricate microarchitecture and scaffolds for stem cell differentiation. Selective laser sintering in particular is simple, amenable to processing a variety of powder materials and finds wide application in the construction of polymer, metal and ceramic scaffold structures for tissue engineering [3]. The powder based AM technique is used to enhance bone regeneration in fabricated tissues and also to develop scaffolds with controlled porosity allowing for the ingrowth of blood vessels [4].

Specific polymers, ceramics, metals, polymer-ceramic composites and metal-polymer composites have been processed by SLS. Both semi-crystalline and amorphous polymers are attempted through SLS and the variations in the thermal characteristics lead to varying process conditions [5]. The glass transition temperature, T_g and the melting temperature T_m play significant roles in controlling the laser sintering aspects [6]. In the case of semi-crystalline polymers, the envelope and the actual sintering temperatures could be close to the glass transition and melting temperatures respectively, while in the case of amorphous polymers, the two are maintained slightly below and above the glass transition temperature [7]. Ceramic materials can be directly laser processed at higher powers, but it is closer to laser melting and involves excessive heating, embrittlement of the substrate and associated issues [9]. The indirect method involves use of polymer-ceramic composites in which the polymer is sintered to serve as the matrix material [8]. In the context of biomedical engineering and in particular bone repair and replacement activities, sintering polymers and ceramics together becomes significantly useful, as the polymer matrix often provides the necessary strength while the ceramic counterpart adds bioactivity. Overall, the composite should offer good

biocompatibility, bioresorbability and processability for applications in either tissue engineering or cartilage repair. Further, the ability to apply an additive manufacturing method such as SLS brings the freedom to reproduce complexity in shapes, a common feature of most biomedical applications.

Selective laser sintering research employing biomaterials in general considered Polycaprolactone (PCL), Polyethylene (PE) Poly-lactic acid (PLA) with Hydroxyapatite (HA) and Tricalcium Phosphate (TCP) targeting scaffolds of lower stiffness and higher resolution of features. PCL scaffolds were fabricated at 300-400 kPa stiffness (lower) allowing for soft tissue engineering applications such as the cardiac tissue [10], while higher stiffness ranges from 14.9-113.4 MPa were also shown to be possible [11]. Considerable amount of work was also done with PCL+HA, PCL+ β -TCP with collagen coatings, and also PLLA+Ca-P composites, demonstrating encapsulation of biomolecules [12]. Shi et al [13] proved that the density and precision of SLS fabricated parts are affected with the particle size of the powder. If the powder has low compaction forces then the parts produced will be porous, and the sintering process results in connected porosity which is a key property requirement for biomedical applications, such as artificial bones and tissue engineering. Williams et al [14] designed and fabricated a polycaprolactone part with controlled porosity at 1.75mm in diameter for biomedical applications and also proved the material to be similar to bone materials in terms of porosity and bioresorbability. Pure Polymethyl Methacrylate (PMMA) as well as PMMA+ β -TCP composites were investigated earlier by the authors [15, 16] and proved to be suitable for processing by selective laser sintering with appropriate combinations of process parameters. Based on morphologies of single layer samples, it was noted that the inter-particle coalescence varies significantly with varying process conditions laser power and velocity. Optimum process conditions were established based on the relationships between the degree of porosity and the process parameters with both pure PMMA [15] and PMMA+ β -TCP composites [16].

The scanning electron microscopy results of the PMMA+ β -TCP composite samples indicated significant variations in the single layer morphologies resulting from varying amounts of β -TCP included in the polymer, within the range 0 to 20%. For a given set of laser power and velocity and when the scan strategy remains the same, these variations could be attributed to the thermal changes induced by the inclusion and dispersion of the β -TCP particles. Since the physical process parameters of SLS associate with the complex modes of heat and mass transfer, the time-dependent temperature distribution within the sintered zones becomes quite critical. Zhang et al [17] have developed an analytical model to theoretically investigate the melting behaviour of subcooled powder bed with mixed powders and obtained temperature distributions in both liquid and solid phases. It was noted that strong energy transformation, momentum transformation and mass transformation produce thermal variations during selective laser sintering process due to the thermal interactions between the laser source and the conditions of the melt pool such as heat conduction and convection and mass transfer. The final quality of products depend on the range and transient nature of the temperature fields in the sintered substrate. Greco and Maggezzoli [18] investigated the melting and sintering behaviour of recycled high-density polyethylene using Differential scanning calorimetry and thermomechanical analysis. Their results indicate that the temperature distribution is governed by the distribution of the crystallinity in the lamellae and the rate of sintering being affected by the variation in the viscosity.

The foregoing literature review and discussion clearly indicate the strong relationship between the thermal fields and the nature of the sintered material. Considering that the thermal properties of PMMA and β -TCP are widely different, it is apt to assume that the thermal

conditions vary with varying amounts of the ceramic component added to the biopolymer. It becomes important to establish the relationships between the morphological changes and the thermal variations that induce these changes with varying compositions of the composite material. The research presented here targets this through experimental and numerical evaluation of the thermal fields of sintered PMMA+ β -TCP powder composite substrates.

II. Materials and Methods

The authors conducted sintering tests and morphological studies on a PMMA+ β -TCP composites earlier and reported elsewhere [16]. However, when fresh powders are obtained from other vendors, the responses were found to be widely different from the previous results, for similar grades of the two constituents, probably due to the long shelf-life of the materials used earlier. For this reason, some of the tests are repeated and reproduced here, with the new powder material combinations. The PMMA (C₅O₂H₈) powder is purchased from Aldrich chemicals with particle size averaging at around 75 μ m. The melting and glass transition temperatures are 160°C and 106°C respectively and the theoretical density is 1180 kg/m³. The β -TCP [Ca₃(PO₄)₂] powder is also procured from sigma Aldrich chemicals and has a molecular weight of 310.18 g/mol. For the current sintering trials, the β -TCP particles are physically mixed with the PMMA varying the amount of β -TCP from 5% to 20% by weight. The PMMA acts as the matrix polymer in this case. Experiments are conducted using a 60W CO₂ laser together with a powder feed mechanism. The envelope temperature is simulated by means of a hot plate substrate arrangement associated with a temperature controller. Scanning electron microscopy is employed for the morphological studies. The key element of SLS process control to understand the effects and interactions of the main fabrication parameters on the composite material system is the incident energy. The applied energy density can be evaluated using Equation 1 which is the most widely used relationship for predicting the critical responses of the SLS process.

$$ED = \frac{P}{D*v} \left(\frac{J}{mm^2} \right) \quad (1)$$

Where P is the laser power, D is the beam diameter and v is the laser beam velocity

An infrared measuring system is employed for recording the transient temperature variations at different points along the length of a single track laser sintered line on a uniformly spread polymer composite powder substrate. The radiant intensity is different with different surface temperatures, and the radiant wavelength is also different, but the infrared waves are always included and so the measurement is reasonably reliable. However, it is important to trace the laser and record the transient temperature distribution at different points along the scan direction. In the current research, the presence of the relatively highly conductive β -TCP particles in the low conducting PMMA substrate will play some role, which needs to be captured accurately.

III. Morphologies of sintered samples and Mechanical testing

PMMA- β -TCP composite materials with varying compositions like 5% β -TCP/ 95% PMMA, 10% β -TCP/ 90% PMMA, 15% β -TCP/ 85% PMMA, 20% β -TCP/ 80% PMMA are evaluated, with particle sizes at 5 to 10 μ m (β -TCP) and 70 to 100 μ m (PMMA). Initial sintering trials allowed narrowing the ranges for power 34W to 42W and the scan speed 450 to 810 mm/s.

With laser power and scan speed varied within these ranges, three specific energy densities are identified for the initial experiments as listed in Table 1. Qualitative observations are made based on SEM photomicrographs of sintered single layer samples with process conditions as given in Table 1. The surface of the sintered sample of 5 % β -TCP/ 95% PMMA for energy density 0.08 J/mm^2 showed a much bigger heat affected zone when increasing the laser power from 34W to 42W, with samples gradually turning from brown to black and at the end dissipating a black smoke, indicating polymer decomposition. Apparently, the base polymer is carbonised in the presence of β -TCP, as the power input is gradually increased. However, the particle fusion and the inter-road coalescence are better at relatively lower power settings. When the β -TCP level is increased from 5% to 10%, drastic changes occurred in the sintered specimens as the porosity levels increased and at higher power, the surfaces looked quite irregularly shaped. With further increase in β -TCP to 15% and 20% and processed at 0.08 J/mm^2 , the pore sizes also increased clearly indicating lack of fusion between adjacent laser scan lines and insufficient formation of the sintered layer. The presence of β -TCP makes the polymer to agglomerate in clusters, along each scan line. The 20% β -TCP sample actually caught fire at 42W laser power, while the 34W and 450mm/s power and speed setting worked fine.

Similar observations were noted with the 0.1 J/mm^2 energy density as the heat affected zone increases with increasing energy density and the specimens begin to decompose at higher power settings, which is also much more pronounced at higher β -TCP levels. The surface colour of the sintered sample gradually becomes brown and the sizes of pores increase. Though inter particle sintering was reasonable at lower power settings, there is still lack of fusion between the lines though the results are better compared to specimens sintered at 0.08 J/mm^2 with 5% and 10% of β -TCP. With the energy density at 0.15 J/mm^2 , the lower power range resulted in improper fusion between adjacent scan lines while higher laser power settings resulted in better inter-strand fusion. The porosity levels and surface irregularities increased with higher β -TCP contents, at above 15 and 20%, while the 20% of β -TCP resulted in excessive particle agglomerations.

Table 1 Laser Process Parameter

Energy Density J/mm^2	Power W	Speed mm/s
0.08	34	750
	38	780
	42	810
0.1	34	650
	38	680
	42	710
0.15	34	450
	38	480
	42	510

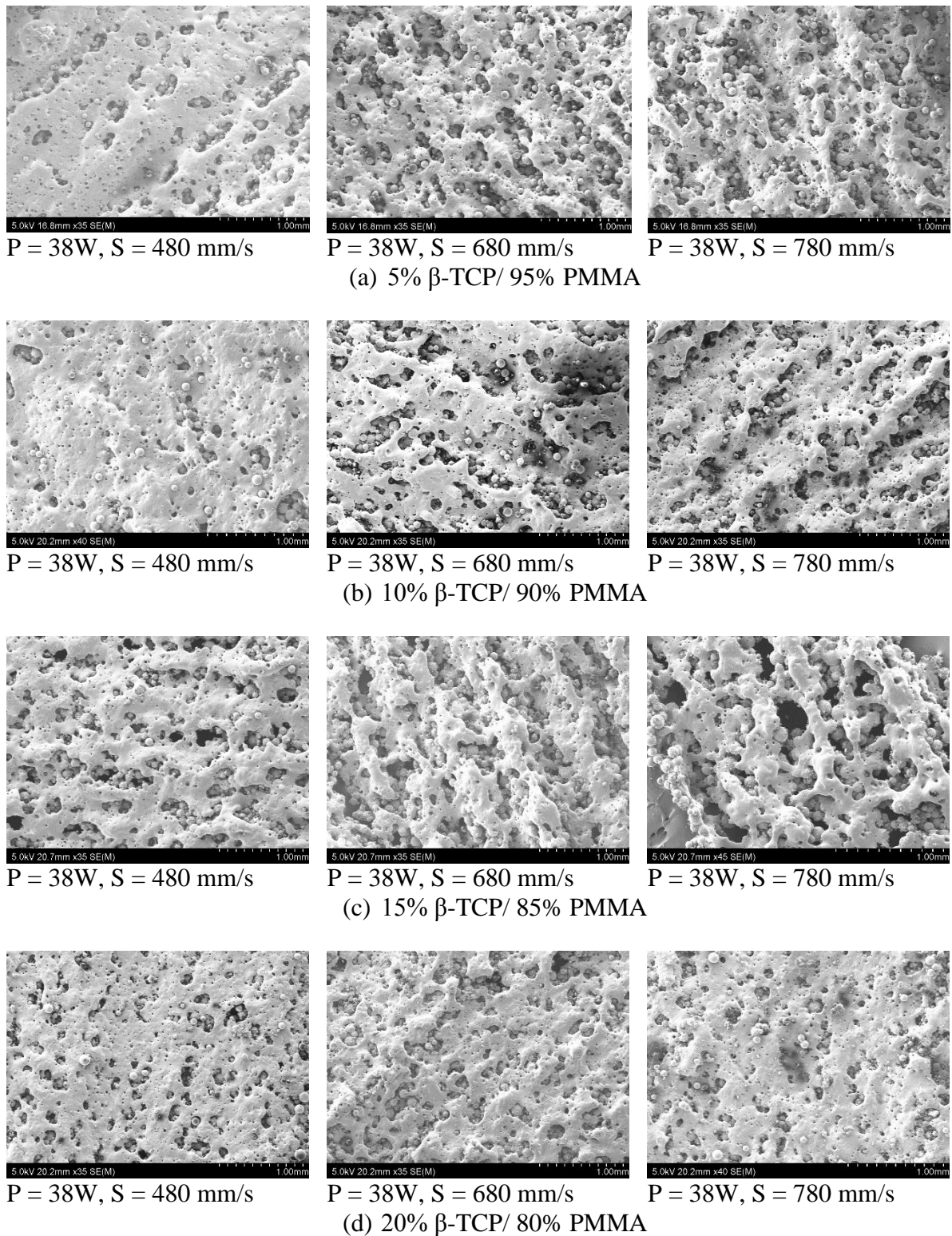


Figure 1 SEM photomicrographs of sintered PMMA- β -TCP composite materials

Based on these initial tests, the most promising laser power range is identified to be around 38 W, while the laser scan speed could be varied at 480 mm/s, 680 mm/s, and 780 mm/s, so as to achieve the three energy density settings as listed in Table 1. SEM images are taken based on samples sintered with these parameter settings and are presented in Figure 1 for varying

compositions of PMMA+ β -TCP composites. The surface morphologies indicate waviness, due to the interaction time between the laser beam and the powder particles. The presence of the relatively smaller β -TCP particles adversely affected the plastic flow and perhaps the liquid as well as the solid state sintering. While the level of sintering within the layer deteriorates with increasing scan speed, the 5% and 10% β -TCP cases show better sintering compared to the 15% and 20% cases.

Further, the porosity level within the polymer matrix also increased with increasing β -TCP as shown in Figure 2. The number of pores as well as their sizes increased with increasing β -TCP. While the physical size variations between the particles of the two constituents could be a plausible cause, it is mainly the thermally inactive β -TCP absorbed within the plasticised PMMA and the consequent reduction in the viscous flow of the plasticised material that could have caused this loss of coalescence. An optimum appears to exist at higher energy density levels, and within the lower levels of β -TCP, for which the intra-layer coalescence is improved as shown in Figure 1. These observations clearly elucidate that the surface morphology and the pore size can be modified by varying the laser parameters together with the composition, allowing for controlled biological responses required in bio-medical applications. This surface porosity will provide the required topology for cell ingrowth into implant and the β -TCP helps with the osteoconductivity.

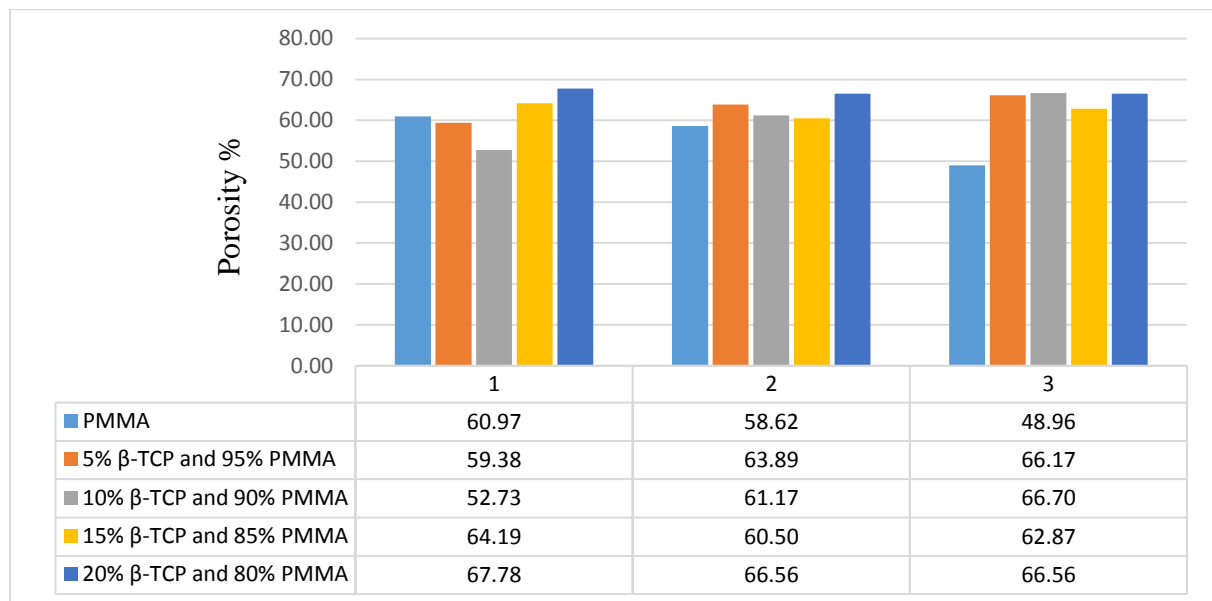


Figure 2 Percent porosity variation with varying amounts of β -TCP

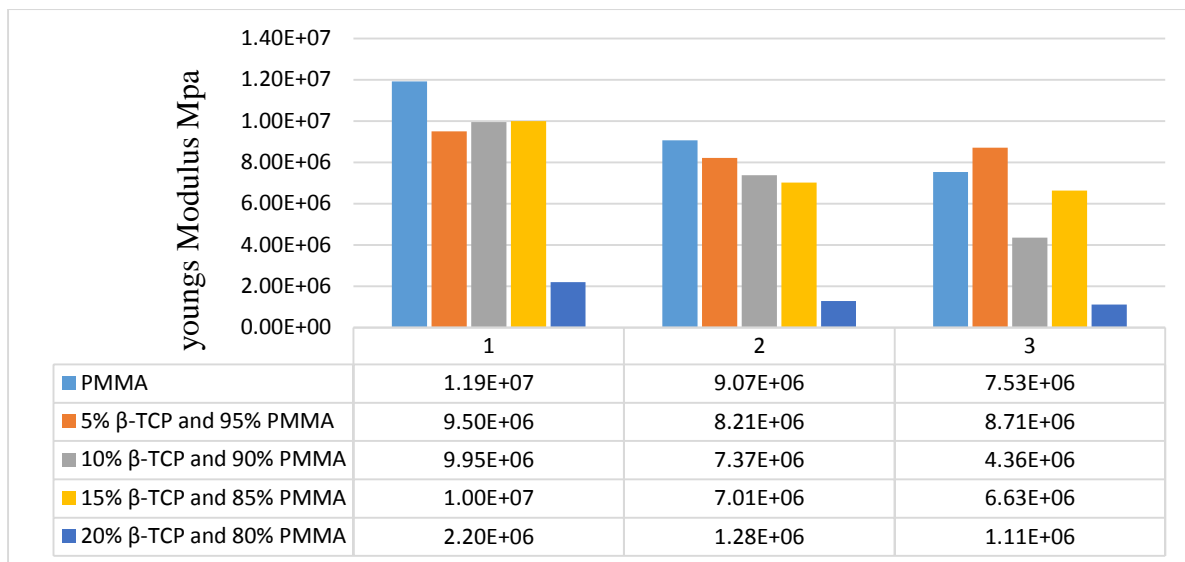


Figure 3 Variation in the Young's Modulus with varying amounts of β -TCP

Thin film tensile tests are conducted as per the ASTM standards, based on the single layer samples sintered with varying process conditions and compositions. The variation in the Young's Modulus values is in similar lines to the porosity variation, as shown in Figure 3. The 20% β -TCP case resulted in a lower elastic modulus, compared to the 5% β -TCP case, as the porosity levels increased resulting in insufficient consolidation within the layers. Similar results were noted by Beruto et al. [19] for TCP/PMMA composites, as the tensile strength significantly decreased with the presence of the bio ceramic component. From the specimens it is observed that the bio ceramic agglomerates during the sintering process, and there is a lack of fusion between adjacent laser scan lines. Considering the thermomechanical nature of consolidation, these changes are plausibly the result of varying thermal conditions emanating from the varying amounts of β -TCP. This will be verified next by numerical and experimental means.

IV. Thermal evaluation

IV a. Finite element simulation

Melting and re-solidification of powder particles leads to the formation of a layer and the inter-layer bonding, in order to create functional parts through the SLS process. Thermal phenomena play dynamic roles in achieving a desired sintering depth, while laser beam radius, laser intensity, scan velocity etc. become critical parameters. However, thermal modelling of the SLS process is more complicated due to various physical processes involved. The finite element method is used here first to simulate the thermal field conditions for a single track laser scanning over the powder bed, evaluating the transient temperature variation at different points along the scan line. Kolossov et al [20] considered the SLS transient temperature variation as a 3D non-linear heat transfer problem and the heat conduction model is expressed using the principle of conservation of energy. This relates the local density of the powder bed during sintering, volume of the powder bed in relation to its surface, heat conduction relating specific heat capacity and position in the space and heat flux density of the laser per area. Thermal conditions like local effective thermal conduction coefficient, convection heat exchange coefficient, pre-heat temperature and emissivity of powder are needed to achieve the

conservation of energy. Considering a CO₂ laser beam as the heat source with a 10.6μm wavelength, the Laser heat flux can be calculated using equation 2 [21].

$$I(r,w) = (1-R_e)I_0 \exp\left(-\frac{2r^2}{w^2}\right) \quad (2)$$

Where r is radiation distance; R_e is the reflectivity of powder surface; w is the characteristic radius; I_0 is the maximum light intensity, which is decided by laser power and characteristic radius of laser.

The finite element simulation is carried out using ANSYS academic research module, considering a 2D domain of 50mm X 20mm dimensions using the four-node quadratic element (PLANE55). The effective thermal conductivities and the densities of various compositions of PMMA+β-TCP are determined based on the weight percent ratios. The following are some of the other assumptions:

- The input heat flux is treated as internal heat generation within the powder layer. Gaussian distributed heat flux is adopted for the heat flux from the laser beam which is given over the powder layer.
- The finite element discretisation is done in such a way that the heat flux due to laser irradiation could be expressed per element, for each location, where the element size is equal to the laser beam diameter 540 μm
- The powder layer is considered to be homogeneous and continuous
- The powder bed temperature is maintained at 90°C and locations where the temperature is more than melting temperature are considered to be sintered.
- The effective thermal conductivity of the powder layer is used for simulation, which incorporates solid thermal conductivity for various volume fractions of the composite material.

The temperature distribution at a particular location during the laser movement over the powder bed is shown in Figure 4. The red spot denotes the laser sintering location, while the temperature distribution indicated the heat affected zone. The time dependent variation in the temperature at a location 20 mm from the start of the laser scan track is shown in Figure 5, for different compositions of the PMMA+β-TCP composite. Evidently, the higher the β-TCP content, the slower the temperature rise as well as the lower the peak temperature. The laser absorptivity appears to be lowered with increased amounts of the bio-ceramic filler. This will in turn affect the viscosity and the liquid and solid state sintering aspects of the powder bed.

IV b. Experimental measurement

An infrared thermal imaging camera is employed for recording the time-dependent temperature variations at different points along the length of the single line laser scan. Figure 6 presents the results of these measurements at 10 equidistant points between the limits 20 mm and 50 mm of the laser travel for three different compositions; pure PMMA, 5% β-TCP/ 95% PMMA and 10% β-TCP/ 90% PMMA. The blue line and the orange lines correspond to the locations at 20 mm and 50 mm from the start of the sintering line respectively, while the other lines correspond to the temperature variations at different intermediate points. Comparing the blue lines across the three cases presented in Figure 6, it is clear that the temperature rise at the 20 mm location is considerably delayed with increasing β-TCP content, ascertaining the observations made from the numerical solution.

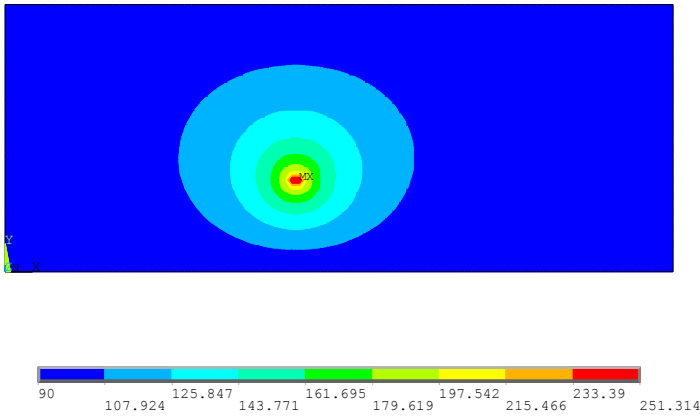


Figure 4 Temperature distribution at a specific time
 $P = 38W$, speed = 780mm/s

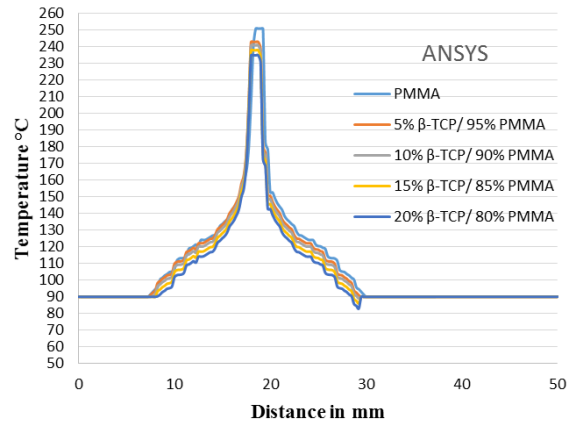


Figure 5 Time dependent temperature variation at 20mm with varying compositions

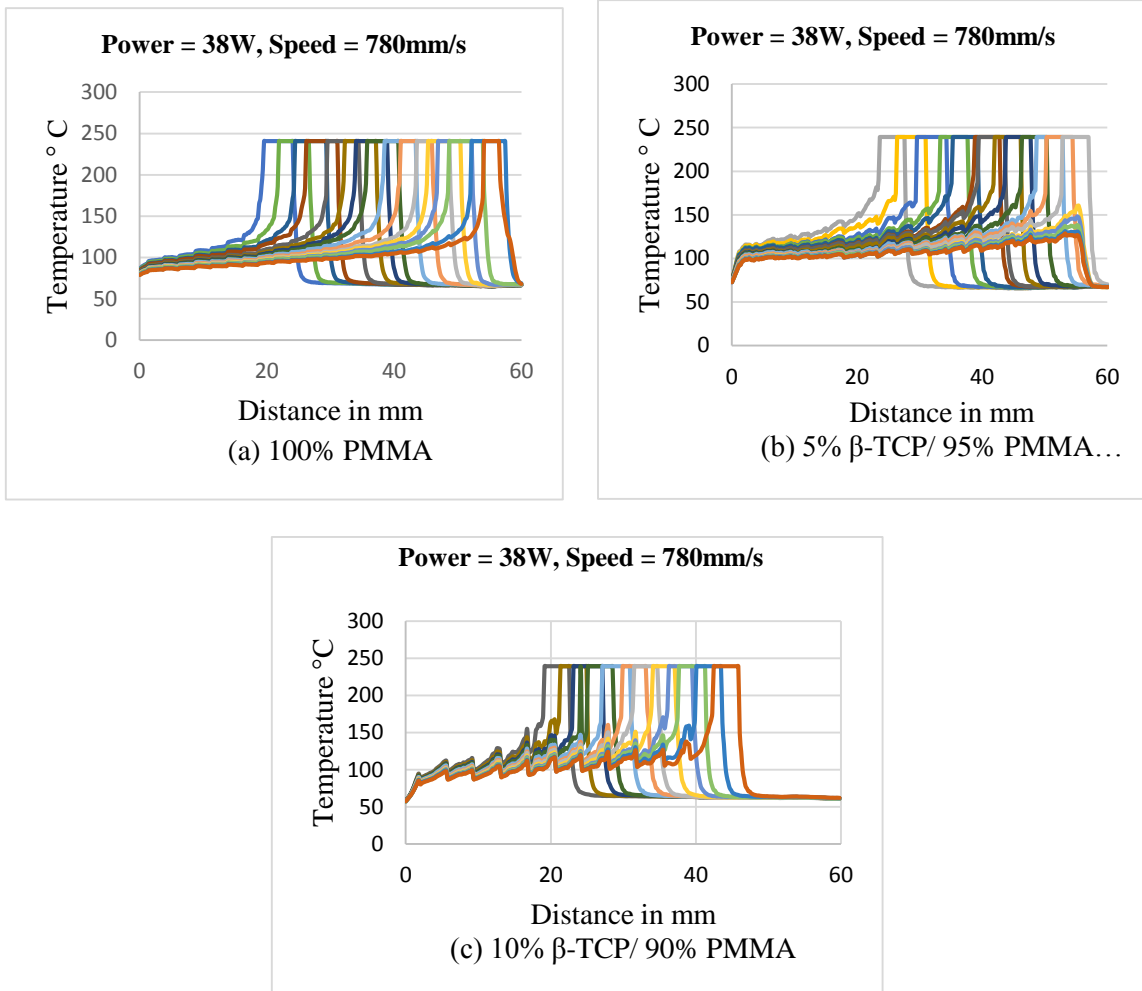


Figure 6 Infrared thermal imaging results of the time dependent variation in temperature at different locations for varying compositions

However, a close observation of the results presented in Figure 6 reveals the significant role of the ceramic filler in altering the temperature variations at different points. With the pure PMMA case, each point gets heated up to the maximum temperature at around 248 °C, with almost similar temperature-time profiles. The phase lag between adjacent lines is due to the time difference experienced by the laser, while passing through the successive points. As the β -TCP content is increased to 5% and then 10%, it may be noted that there is a significant delay in reaching the maximum temperature for the start point, while there is an accelerated temperature rise at later points. The time delay in raising the temperature at a specific location is in accordance with the numerical results, probably indicating an overall drop in the laser absorptivity of the powder composite with increasing amounts of the loaded ceramic, as most heat is actually absorbed by the ceramic component. The accelerated temperature rise at specific locations and perhaps even before the laser actually reaches them could be due to an increased conduction of heat through the powder bed at higher contents of β -TCP. These cycles are associated with corresponding thermal stress changes [22]. While the peak temperature varied from 235–251°C as predicted by the FE model for varying compositions, the experimental results did not show appreciable variation in the peak temperature with composition. However, it is clear from both the numerical simulation and the experimental observations that the β -TCP component absorbs the laser energy faster and results in a dominant thermal energy transfer through conduction and in fact, the 20% of β -TCP cases begin to burn, char and decompose with laser power at 38 W and above as evidenced from some of the photomicrographs of the initial trials.

V. Conclusion

PMMA and Beta Tri-calcium Phosphate composites are evaluated for processing through selective laser sintering. Photomicrographs of single layer samples sintered with varying process conditions and compositions showed widely varying morphologies. Considering the thermal nature of material consolidation mechanisms, these variations are attributed to changes in the thermal fields, resulting from the varying amounts of the bio-ceramic filler material. Both numerical simulations and experimental measurements proved this to be true and the following are the specific conclusions:

- The laser sintering process effective in building well coalesced layers at relatively low levels of β -TCP (less than 10%) and lower laser power settings (around 38 W).
- The higher the β -TCP content, the more the porosity and the larger the pore sizes.
- The overall laser absorptivity of PMMA+ β -TCP composite reduces as the filler ceramic content increases.
- The higher the amount of β -TCP, the larger is the tendency for the heat to be transferred by conduction.

References

1. Hutmacher D W, Sittinger M and Risbud M V 2004 Scaffoldbased tissue engineering: rationale for computer-aided design and solid free-form fabrication systems Trends Biotechnol. 22 354–62
2. Pham D T and Gault R S 1998 A comparison of rapid prototyping technologies Int. J. Mach. Tools Manuf. 38 1257–87

3. Rahmati S, Abbaszadeh F and Farahmand F 2012 An improved methodology for design of custom-made hip prostheses to be fabricated using additive manufacturing technologies *Rapid Prototyping J.* 18 389–400
4. Bohner M, van Lenthe G H, Grunenfelder S, Hirsiger W, Evison R and Muller R 2005 Synthesis and characterization of porous beta-tricalcium phosphate blocks *Biomaterials* 26 6099–105
5. Ajoku U, Hopkinson N and Caine M 2006 Experimental measurement and finite element modelling of the compressive properties of laser sintered Nylon-12 *Mater. Sci. Eng.: A* 428 211–6
6. Bicerano J and Seitz J T 1996 Molecular origins of toughness in polymers *Polymer Toughening* (New York: Dekker) pp 1–59
7. Kruth J P, Levy G, Klocke F and Childs T H C 2007 Consolidation phenomena in laser and powder-bed based layered manufacturing *CIRP Ann—Manuf. Technol.* 56 730–59.
8. Hagedorn Y C, Balachandran N, Meiners W, Wissenbach K and Poprawe R 2011 SLM of net-shaped high strength ceramics: new opportunities for producing dental restorations *Proc. Solid Freeform Fabrication Symp.* (Austin, TX) pp 8–10
9. Shahzad K, Deckers J, Kruth J-P and Vleugels J 2013 Additive manufacturing of alumina parts by indirect selective laser sintering and post processing *J. Mater. Process. Technol.* 213 1484–94
10. Yeong W, Sudarmadji N, Yu H, Chua C, Leong K, Venkatraman S, et al. Porous polycaprolactone scaffold for cardiac tissue engineering fabricated by selective laser sintering. *Acta Biomater.* 2010; 6:2028–34.
11. Liao HT, Lee MY, Tsai WW, Wang HC, Lu WC. Osteogenesis of adiposederived stem cells on polycaprolactone- β -tricalcium phosphate scaffold fabricated via selective laser sintering and surface coating with collagen type I. *J Tissue Eng Regenerative Med.* 2013.
12. Duan B, Wang M, Zhou WY, Cheung WL, Li ZY, Lu WW. Three-dimensional nanocomposite scaffolds fabricated via selective laser sintering for bone tissue engineering. *Acta Biomater.* 2010; 6:4495–505.
13. Shi, Y., Li, Z., Sun, H., Huang, S., and Zeng, F. Effect of the properties of the polymer materials on the quality of selective laser sintering parts. *Proc. Instn Mech. Engrs, Part L: J. Materials: Design and Applications*, 2004, 218, 247–252.
14. Williams, J. M., Adewunmi, A., Schek, R. M., Flanagan, C. L., Krebsbach, P. H., Feinberg, S. E., Hollister, S. J., and Das, S. Bone tissue engineering using polycaprolactone scaffolds fabricated via selective laser sintering. *Biomaterials*, 2005, 26, 4817–4827.
15. Rajkumar Velu and Sarat Singamneni, “Evaluation of the influences of process parameters while selective laser sintering PMMA powders”, *Proceedings of the Institution of Mechanical Engineers, Part C: Journal of Mechanical Engineering Science*, Vol. 229(4) 603–613, and June 5, 2014.
16. Rajkumar Velu and Sarat Singamneni (2014). Selective laser sintering of polymer biocomposites based on polymethyl methacrylate. *Journal of Materials Research*, 29, pp 1883-1892. doi:10.1557/jmr.2014.211.
17. Zhang, Y., Faghri, A., 1999. Melting of a subcooled mixed powder bed with constant heat flux heating. *International Journal of Heat and Mass Transfer* 42, 775–788.
18. Greco, A., Maffezzoli, A., 2003. Polymer melting and polymer powder sintering by thermal analysis. *J. Therm. Anal. Calorim* 72, 1167–1174.
19. Beruto DT, Mezzasalma SA, Capurro M, Botter R, Cirillo P. Use of a-tricalcium phosphate (TCP) as powders and as an aqueous dispersion to modify processing,

- microstructure, and mechanical properties of poly (methyl methacrylate) (PMMA) bone cements and to produce bone-substitute compounds. *J Biomed Mater Res* 2000; 49:498–505.
20. Kolossov, S., Boillat, E., Glardon, R., Fischer, P. and Locher, M. (2004), 3D FE simulation for temperature evolution in the selective laser sintering process, *Int. J. Mach. Tools Manuf.*, Vol. 44, pp. 117-23.
 21. B. Zhao, F. Shi, T. Feng, et al., Studies on numerical simulations of temperature field in selective laser sintering of polystyrene powders, *Laser J.* 23 (2002) 66–69.
 22. K. Dai, L. Shaw, Distortion minimization of laser-processed components through control of laser scanning patterns, *Rapid Prototyping Journal* 8(5) (2002) 270–276.